Bio-Design and Manufacturing (2023) 6:550–562
https://doi.org/10.1007/s42242-023-00251-5

RESEARCH ARTICLE

3D bioprinting of complex biological structures with tunable elastic modulus and porosity using freeform reversible embedding of suspended hydrogels

Zhuang Chen[1] · Chuanzhen Huang[2] · Hanlian Liu[1] · Xu Han[1] · Zhichao Wang[1] · Shuying Li[1] · Jun Huang[1] · Zhen Wang[2]

Received: 19 December 2022 / Accepted: 14 June 2023 / Published online: 12 July 2023

Abstract

Three-dimensional (3D) bioprinting has been used widely for the construction of hard tissues such as bone and cartilage. However, constructing soft tissues with complex structures remains a challenge. In this study, complex structures characterized by both tunable elastic modulus and porosity were printed using freeform reversible embedding of suspended hydrogels (FRESHs) printing methods. A mixture of alginate and gelatin was used as the main functional component of the bioink. Rheological analysis showed that this bioink possesses shear thinning and shear recovery properties, supporting both cryogenic and FRESH printing methods. Potential printing capabilities and limitations of cryogenic and FRESH printing were then analyzed by printability tests. A series of complex structures were printed by FRESH printing methods which could not be realized using conventional approaches. Mechanical tests and scanning electron microscopy analysis showed that the printed structure is of excellent flexibility and could be applied in various conditions by adjusting its mechanical modulus and porosity. L929 fibroblast cells maintained cell viability in cell-laden-printed structures, and the addition of collagen further improved the hydrogels' biocompatibility. Overall, all results provided useful insight into the building of human soft tissue organ blocks.

✉ Chuanzhen Huang
huangchuanzhen@ysu.edu.cn

[1] Centre for Advanced Jet Engineering Technology (CaJET), Key Laboratory of High-Efficiency and Clean Mechanical Manufacture (Ministry of Education), National Experimental Teaching Demonstration Center for Mechanical Engineering (Shandong University), School of Mechanical Engineering, Shandong University, Jinan 250061, China

[2] School of Mechanical Engineering, Yanshan University, Qinhuangdao 066004, China

Graphic abstract

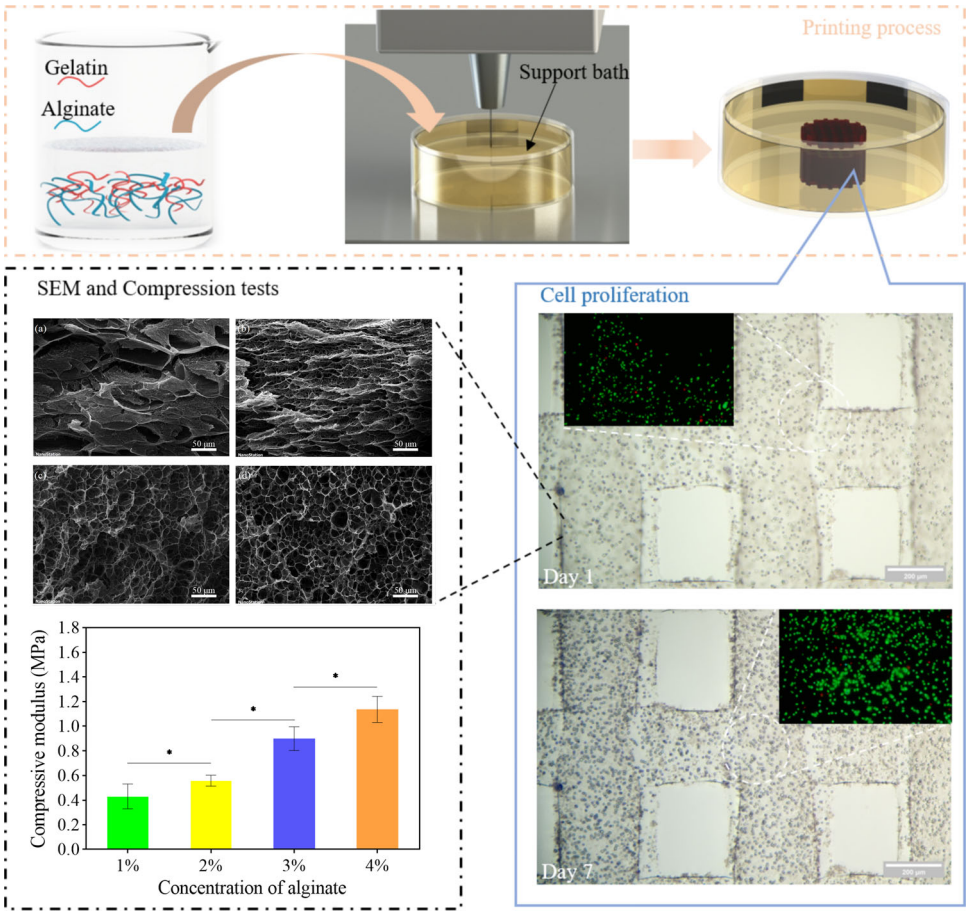

Keywords Bioink · Freeform reversible embedding of suspended hydrogels (FRESHs) printing · 3D extrusion cell-laden printing · Tissue engineering · Tunable elastic modulus and porosity

Introduction

Donor transplantation, the most effective treatment for organ necrosis, still suffers from a shortage of global sources [1]. Due to the scarcity of organ banks, fewer than 1/3 of patients on waiting lists in the USA are able to receive organ transplants each year, and more than 100,000 people die from end-stage organ disease [2, 3]. Recent reports claim that some transplant centers in the USA are proposing to allow transplants only for patients who have received COVID-19 vaccination, making organ transplant donors even more stressed [4].

Tissue engineering is currently one of the most promising techniques to alleviate the shortage of organ transplant donors [5]. At present, three-dimensional (3D) bioprinting technology is booming and has been widely used for the printing of bone tissues [6]. In addition, 3D bioprinting has made important progress in the construction of complex tissues such as vascularized bone tissue [7], liver [8], cardiac [9], and kidney [10]. 3D bioprinting is expected to be an effective method to solve organ shortages. Hydrogels are considered the most promising bioink materials due to their similarity to the extracellular matrix (ECM) [11–14]. Nevertheless, these biomaterials require high concentrations to maintain the stability of the printed structures, making it difficult to print soft tissues with complex structures [15]. The use of low-concentration bioink is a standard method of constructing soft tissues [16]. However, this method has intrinsic drawbacks due to the high loss modulus and the slow cross-linking of this bioink [17]. Under gravity, the cylindricity of the extruded filament will change, and the printing structure will gradually collapse with the increase in printing layers [18, 19]. Another approach is to print soft tissues with composite structures using polymeric biomaterials and

natural materials as structural support and cell-laden bioink, respectively [20]. This strategy combines both mechanical properties and biocompatibility, but polymeric materials still present potential biotoxicity and degradation difficulties.

Freeform reversible embedding of suspended hydrogels (FRESHs) is an effective solution for constructing soft tissues due to its ability to overcome gravity in the printing process [21]. The FRESH printing principle exploits Bingham fluid yielding properties [22]. Specifically, FRESH extrudes bioink into a support bath with Bingham fluid properties, which locks the extruded bioink in 3D space during printing. Upon completion of the printed structure, the support bath warms up and liquefies to release the printed material. The FRESH method has been studied to achieve the printing of polymers such as polydimethylsiloxane, polyethylene glycol, and silicone [23–25]. In recent years, FRESH has also been used in 3D bioprinting. Lee et al. [26] successfully printed a mini heart using the FRESH printing method, with heart tissue using collagen as the external scaffolding material and human stem cell-derived cardiomyocytes as the internal filling. The printed heart can perform pumping functions, showing the great potential of the FRESH approach. Furthermore, Mirdamadi et al. [27] used the FRESH method to construct full-size human hearts with the mechanical properties of human heart tissue. Unfortunately, due to the long printing time, it does not support cell-laden printing. A recent study proposed a six-axis robot combined with FRESH printing capable of generating vascularized, contractible, and long-term surviving cardiac tissues [28]. In addition, FRESH supports the printing of various tissues, such as cartilage [29], skeletal muscle [30], and blood vessels [31]. Overall, FRESH printing shows great advantages and demonstrates huge potential. However, there are no studies that quantify the differences between FRESH printing and conventional extrusion-based printing [32]. The elastic modulus and micromorphology of the printed tissues also need to be investigated. Alginate has good biocompatibility and is used as a support component in biological scaffolds to modulate the elastic modulus [33]. Although alginate has been investigated for the FRESH printing method [31], printing with a single component of alginate can lead to reduced accuracy due to the diffusive nature of alginate [34, 35]. Gelatin is a thermoreversible material that is widely used for extrusion-based printing [36]. This study uses gelatin to improve the printability of alginate and to regulate the scaffold porosity as a sacrificial material.

In this work, bioinks with tunable porosity and mechanical properties were designed and prepared for extrusion printing in a gelatin particle support bath using the FRESH method. In brief, a series of gelatin/alginate bioinks with different component contents were first configured, and a gelatin support bath slurry was prepared by mechanical crushing methods. To analyze the printability, the rheological properties were measured using a rheometer, and the extrusion state of the ink was further analyzed by simulation. In addition, the mechanical properties and porosity of the hydrogel were examined by mechanical and scanning electron microscopy (SEM) tests. The FRESH process was optimized to build a series of complex structures. Finally, cell-laden scaffolds were printed, and cell viability was further improved by adding specific cell-additive materials—collagen.

Materials and methods

Material preparation

Gelatin was purchased from Macklin Biochemical Co., Ltd. (Shanghai, China). Sodium gelatin, $CaCl_2$, and carmine were purchased from Sigma–Aldrich (Shanghai, China). Phosphate-buffered saline (PBS) was purchased from Solarbio Science & Technology Co., Ltd. (Beijing, China). Minimum essential medium (MEM) and L929 mouse fibroblast cells were purchased from Meilun Biotechnology Co., Ltd. (Suzhou, China). Fetal bovine serum (FBS) was purchased from Biological Industries Israel Beit Haemek Ltd. (Haifa, Israel). Penicillin/streptomycin (P/S) was purchased from Gibco Inc. (Grand Island, USA).

The extruded bioink was prepared by dissolving a range of gelatin and sodium alginate powders in 1× PBS at 37 °C and stirring for 2 h. Subsequently, sterilization was performed using a 0.22-μm filter. The cell suspension was mixed with degassed bioink to obtain a cell concentration of 1×10^6 mL^{-1}. Alternatively, carmine (0.0005 g/mL) could be added to the extruded bioink to visualize the printing process. The support bath ink was a Bingham fluid composed of gelatin and $CaCl_2$. Specifically, 5% (0.05 g/mL) gelatin granules and 0.1% (0.001 g/mL) $CaCl_2$ powder were dissolved in ultrapure water, followed by stirring at 37 °C for 30 min to make the dispersion homogeneous. The configured solution was cured overnight at 4 °C. Subsequently, the cured colloid and 0.1% $CaCl_2$ solution were added to a commercial mixer (L3-C8, Joyoung Company Limited, China) at a ratio of 1:3 for crushing. The gelatin particles with 0.1% $CaCl_2$ solution were washed until there was no foam in the upper layer. Finally, the desired support bath was obtained by centrifugation and compaction.

Rheology evaluation

The rheological properties of bioinks were measured using an Anton Paar MCR 302 rheometer (Graz, Austria) equipped with a 25-mm diameter, 2° cone plate. The viscosity profile of the bioink was tested at 37 °C. Each specimen was scanned at a shear rate of 0.1 to 100 s^{-1} slope. The shear thinning property of the bioink was characterized by measuring the

viscosity (η). For non-Newtonian fluids, the viscosity can be derived from the power law equation:

$$\eta = K\dot{\gamma}^{n-1}, \tag{1}$$

where η is the viscosity of non-Newtonian fluid, $\dot{\gamma}$ is the shear rate, K is the viscosity index determined by the concentration and temperature of the fluid, and n is a power function exponent or fluidity behavior index. The parameters K and n were determined by shear rate scanning experiments. The shear stress inside the needle was determined by

$$\tau = \eta\dot{\gamma}. \tag{2}$$

Subsequently, the flow state of the ink inside the needle was simulated using ANSYS Fluent. It was assumed that the bioink was an incompressible fluid, and the flow state was laminar, ignoring the effect of gravity and inertia forces.

The gel kinetics of bioinks were evaluated by temperature scanning. The experiments were conducted at 1% strain and 1-Hz frequency. The temperature scanning range was set from 4 to 37 °C, and the scanning speed was set to 5 °C/min. The change process of the storage modulus (G') and loss modulus (G'') of the bioink was measured in both the warming and cooling stages. In addition, the gel underwent a process of a high shear rate in the nozzle and a low shear rate after extrusion during the printing process. Altering high and low shear rate scanning experiments was performed to evaluate the thixotropy of the gel during printing. Specifically, the bioink flow in the syringe was demonstrated by applying a low shear rate (0.01 s^{-1}) of 100 s, then a high shear rate (1000 s^{-1}) of 100 s was applied to simulate the bioink flow in the nozzle, and finally, a low shear rate (0.01 s^{-1}) of 100 s was used to characterize the bioink state after extrusion. The whole experimental procedure was repeated three times.

Mechanical test

The mechanical properties of the hydrogel were characterized by a compression test using a universal testing machine (ZLC-2D, Jinan XLC Testing Machine Co., Ltd., China). Specimens were prepared by curing the bioink in a designed cylindrical mold. The specimen shape was a 10-mm high, 10-mm diameter column. The loading rate in the experiment was 1 mm/min, and the compressive displacement was half of the specimen's height. The stress–strain curve was drawn by Origin2019b, and the compression modulus was calculated within the strain range of 10%.

Scanning electron microscopy

To investigate the relationship between the internal polymer network microstructure of hydrogels and the concentration of bioink components, the microscopic morphology of hydrogels was photographed using a JSM-7601F SEM (JEOL, Japan). The hydrogel samples with dimensions of 10 mm in diameter and 10 mm in height were freeze-dried at −50 °C for 24 h. The lyophilized hydrogel was manually broken to expose the internal interface. After performing the gold spraying operation, the sample was fixed on the sample table for observation.

3D bioprinting process

The bioprinter used in this study was a pneumatic-driven 3D bioprinter (EFL-BP-6002, Suzhou, China). The printer was equipped with a cryogenic sprinkler and a cryogenic platform to control the temperature of the extruded bioink and support bath. The extruded bioink was added to the syringe of the printhead, which can print a diameter range of 260 μm to 1.2 mm by combining different sizes of flat needles. A pressure regulator valve above the printer controlled the air pressure of the extruded bioink with an accuracy of 0.1 kPa. The printing effect of bioink was investigated by both cryogenic and FRESH printing methods, as shown in Fig. 1.

In the cryogenic extrusion printing method, the thermoreversible property of gelatin was used for rapid prototype printing. The bioink was incubated in the barrel at 37 °C for 10 min and then printed directly onto a platform at 5 °C. The printed scaffolds were soaked for 5 min using 5% (0.05 g/mL) $CaCl_2$. Finally, the scaffolds were washed three times using 1× PBS and incubated in an incubator with MEM.

The FRESH printing method accomplished scaffold construction by extruding bioink into the support bath. After centrifugation and compaction, the gelatin pellet slurry was uniformly spread over a Petri dish. The control software of the host computer sets the printing parameters. Printing was performed using a 25-G needle with a layer height of 200 μm. The printing speed was 5 mm/s. The platform temperature was set to 20 °C, and the nozzle temperature was set to 37 °C according to the support bath requirements. Model slicing and print path planning were processed by Slic3r, which then sent the generated G-code to the printer. During the printing process, the extruded bioink combined with calcium ions in a gelatin slurry to form ion cross-linking and curing. The printing time depended on the complexity of the model. After printing was completed, the platform temperature was raised to 37 °C to release the printed structures. The scaffolds were soaked for 5 min using a 5% $CaCl_2$ solution and then washed twice with 1× PBS.

Cell activity detection

For the biocompatibility of the printed structures, we conducted cell-loaded printing experiments using L929 fibroblast cells. The printed structures were incubated in a 37 °C,

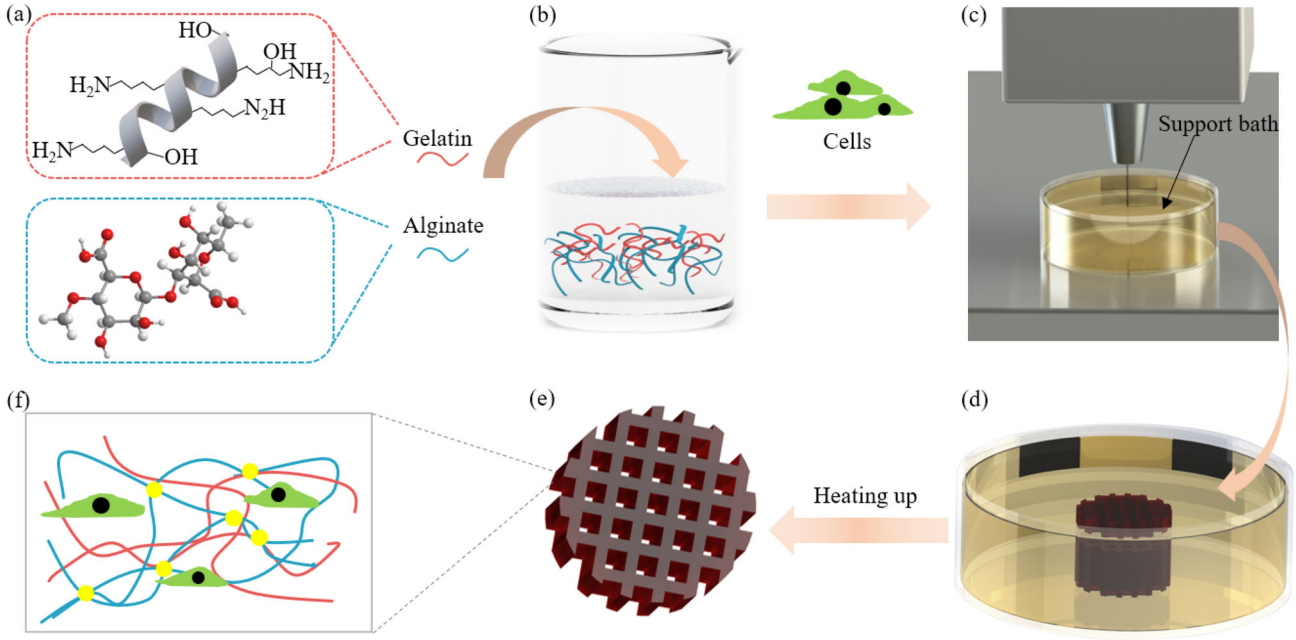

Fig. 1 FRESH 3D bioprinting with tunable elastic modulus and porosity tissues: **a** structural formula of the material used to prepare the bioink; **b** preparation of bioink; **c** FRESH 3D bioprinting process; **d** printed structures preserved in the support bath; **e** scaffold released from the support bath at 37 °C; **f** schematic diagram of the hydrogel's microstructure. FRESH: freeform reversible embedding of suspended hydrogel

5% CO_2 incubator using MEM supplemented with 10% FBS (Gibco) and 1% P/S (Gibco). The culture solution was changed every other day. Cell proliferation was assessed on Days 1, 3, 5, and 7 using the cell counting kit-8 (CCK-8). In addition, cell activity and morphology were evaluated on Days 1 and 7 using live/dead cell stains, where live cells were stained green with calcein acetoxymethyl ester (AM) and dead cells were stained red with propidium iodide (PI). The staining results were observed using an inverted fluorescence microscope.

Statistical analysis

All experiments were repeated at least three times, and the results are expressed as the mean±standard deviation (SD). Statistical analysis was performed by GraphPad Prism. One-way analysis of variance (ANOVA) was utilized to analyze variance with Bonferroni post-tests to compare between groups. Statistical significance was defined as $^{**}p<0.01$, $^{***}p<0.001$, and $^{****}p<0.0001$.

Results and discussion

Rheological properties

Rheological properties of bioink significantly impact printability and cell viability [37]. In this section, rheological properties such as shear thinning, shear recovery, and gel kinetics of different concentrations of bioinks were tested (Fig. 2a). The gel kinetic behavior of bioink was determined by temperature scanning. Gelatin is a soluble protein compound obtained by partially hydrolyzing collagen, which exhibits a liquid-like state above the gelation temperature and becomes a hydrogel state upon cooling [36, 38]. To determine the appropriate printing temperature range, we tested the gel kinetics of bioinks in oscillation mode at a frequency of 1 Hz in the range of 4–37 °C. The bioink concentration ratios and test procedure notation are noted in Table 1. As shown in Fig. 2b, the storage modulus (G') of all bioinks was greater than the loss modulus (G'') at lower temperatures, which indicated that the ink exhibited a solid state; G' was smaller than G'' at higher temperatures, which indicated that the bioink exhibited fluid properties. The intersection of G' and G'' in the hydrogel kinetic curve represented the temperature at which the sol–gel transition of the bioink occurs, which was not the same during the warming and cooling processes, consistent with that of a previous study [39]. T1, T2, and T3 (Fig. 2b) were the differences between the gel and sol temperatures of the three inks. The gel temperature of all bioinks was approximately 10 °C lower than the sol temperature (Table 1). This property indicated that the bioink fully met the printing requirements, since the printed structures remained cured over a wide range of temperatures, which facilitated adequate ionic cross-linking of the printed structures. In addition, experiments showed that the concentration of ink affected the gelation process, and when the concentration of gelatin was below 2%, the gelation temperature of

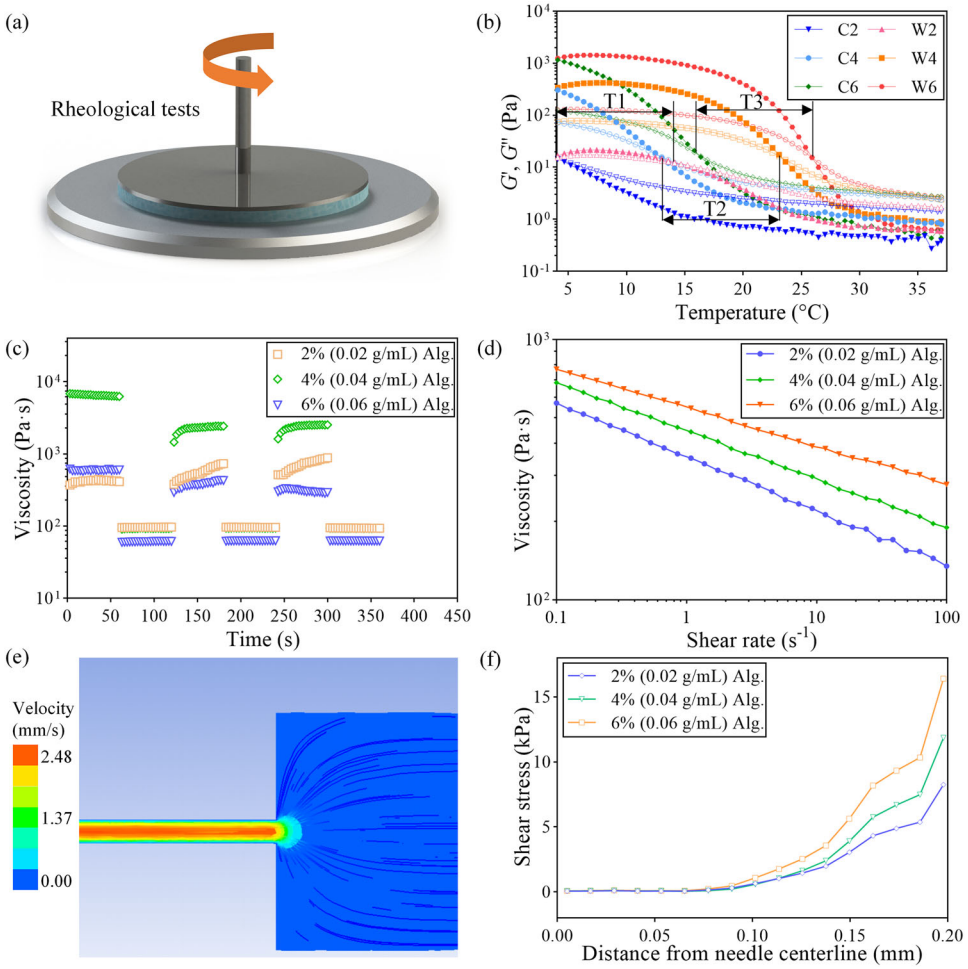

Fig. 2 **a** Schematic diagram of the rheological test. **b** Gel kinetic curves of bioinks containing 2%, 4%, and 6% (0.02, 0.04, and 0.06 g/mL) gelatin during warming and cooling. Legend: solid for G', hollow for G'', W for warming, C for cooling, numbers for gelatin concentration. **c** Mutated high (1000 s^{-1}) and low (0.01 s^{-1}) shear rates over three cycles at 37 °C. **d** Shear rate sweep at 37 °C. **e** Velocity field of bioink flow in the needle. **f** Shear stress of three concentrations of ink in the needle at different radius positions

Table 1 Sol/gel temperature in kinetics testing

Gelatin (g/mL)	Gelling temperature (°C)	Sol temperature (°C)	Temperature difference (°C)
0.02	4.09	14.68	10.59
0.04	12.45	23.09	10.64
0.06	15.24	25.91	10.67

bioink decreased to below 4 °C. Therefore, the bioink was no longer suitable for cryogenic printing when the gelatin concentration was below 2% (0.02 g/mL). The gelatin concentration used in the subsequent rheological experiments was 4% (0.04 g/mL).

The test results on the thixotropy of bioink are shown in Fig. 2c. Mutated high (1000 s^{-1}) and low (0.01 s^{-1}) shear rates were applied to the bioink at 37 °C to simulate the extrusion process of the bioink from the nozzle. The results showed that the viscosity of all concentration ratios of bioink changed dramatically when the shear rate changed abruptly. This property indicated that the bioink passed through the nozzle with low viscosity during the printing process, thus reducing the damage to cells [40]. Once extruded from the nozzle, the bioink flow rate became zero, and the bioink immediately returned to the state of high viscosity, which was conducive to maintaining the structure of the printing. Multiple repetitions of the experiment were performed, revealing that the material maintained good shear recovery behavior, which helped print with good fidelity [15].

The results of the shear scan test on bioink are shown in Fig. 2d. In the shear rate range of 0.1–100 s^{-1}, the shear viscosity of all concentration ratios decreased with increasing shear rate. The test results showed that all samples exhibited shear thinning behavior during printing, which facilitated cell survival [33]. The material characteristics of the bioink—viscosity index K and power law index n—were obtained by fitting the experimental results with MATLAB. Next, the flow state of the bioink in the needle was simulated using ANSYS Fluent. The flow velocity of the bioink in the longitudinal section of the nozzle during the extrusion process was obtained by numerical calculation (Fig. 2e), which showed that the velocity field was flat near the center of the nozzle

and varied sharply near the wall. Figure 2f shows the calculated results of the shear stress in the nozzle cross section along the radius direction. The average shear stresses were 2.00, 2.64, and 3.76 kPa, and the maximum shear stresses were 8.25, 11.85, and 16.41 kPa for the three concentrations of alginate ink containing 2%, 4%, and 6% (0.02, 0.04, and 0.06 g/mL), respectively. The simulation results showed that the bioink had low shear stress in the needle, which would be cell-friendly during the printing process [40].

Elastic modulus

Human tissues have a wide range of elastic moduli, and different types of cells have various modulus requirements. In 3D bioprinting, the elastic modulus of the bioink affects the stability of the printed structure and modulates the growth of cells [41, 42]. Therefore, compression experiments were performed to analyze the elastic modulus of the prepared bioink after curing (Fig. 3a). As shown in Fig. 3b, the elastic modulus of the gel was approximately linearly related to the concentration of alginate. The elastic modulus was (0.430± 0.082) MPa at a concentration of 1% (0.01 g/mL) alginate. As the alginate concentration increased to 4%, the modulus of the gel increased to (1.137±0.087) MPa. The results indicated that mechanically tunable hydrogels can meet the requirements of different cell survival [18, 43]. Compared with most similar material systems in the previous investigation, our research allowed the fabrication of tissue with a low elastic modulus, which was suitable for printing soft tissues such as peripheral nerves and liver [44, 45].

Scanning electron microscopy

The morphologies on the hydrogel cross sections were observed using SEM. As shown in Fig. 4, gelatin concentration had a significant effect on the porosity of the hydrogels. Here, lyophilized hydrogel scaffolds with 2% (0.02 g/mL), 4% (0.04 g/mL), 6% (0.06 g/mL), and 8% (0.08 g/mL) gelatin concentrations were added. The test results demonstrated that when the concentration of gelatin was 2%, the microscopic morphology of the material showed a lamellar shape, and there were no apparent pores (Fig. 4a). As the gelatin concentration increased, the cross-sectional images showed a more uniform microporous structure (the pore sizes in Figs. 4b–4d were (4.48±1.35), (9.74±2.56), and (16.06±4.17) μm, respectively). In addition, porosity increased systematically with increasing gelatin concentration, which was measured to be (34.5±5.7)%, (67.2±3.4)%, and (81.4±2.7)% in Figs. 4b–4d, respectively. This porous structure provided channels for the transport of nutrients and waste excretion and thus facilitated cell proliferation and migration [46, 47]. Some studies have shown that hydrogels prepared by materials such as Poloxamer F127 achieve a similar network of pores and are able to enhance cellular activity [48, 49]. In this study, materials with better cytocompatibility were used to improve the cell survival rate.

3D printability

Printing experiments showed that the bioink could be printed by cryogenic printing and the FRESH printing method, and the print fidelity of the bioink was evaluated by printing multilayer grid structures. After optimizing the printing parameters, multilayer grid structures were printed in the cryogenic platform and support bath. Figure 5 shows the printing results, which demonstrated that the designed structure could be successfully printed using both cryogenic printing and FRESH printing methods. However, due to gravity, the printed structures on the cryogenic platform collapsed more severely with an increasing number of layers (Figs. 5a–5d). Structures printed in the support bath were not affected by gravity (Figs. 5e–5h), so it was not limited to the starting position of the print, which means that the structure can be printed from any point in space.

Furthermore, the print fidelity of the two printing methods was evaluated by defining a function of edge length versus area:

$$S_q = \frac{L^2}{16A}, \tag{3}$$

where L represents the perimeter of the printing structure mesh and A represents the area. For a perfect printing structure, the mesh appears square, and the S_q value equals 1. The value of S_q is smaller than 1 when the mesh shape tends to be circular and larger than 1 when the mesh tends to be irregularly polygonal (Fig. 6a). To determine the S_q value of each printed structure, the perimeter and area of the mesh were measured by ImageJ. The data were analyzed by GraphPad Prism. As seen from Fig. 6b, in low temperature printing, all values of S_q were larger than 1, indicating that the printed mesh edges were irregular. As the number of layers grew, the printing fidelity gradually decreased, and the error increased. In the FRESH printing method, the number of printed layers had no statistically significant effect on fidelity. All S_q values were smaller than 1, which indicated a good printing effect.

Printability experiments demonstrated the characteristics of the two methods when printing the bioinks. Cryogenic printing had a simple printing process and could print cell-laden scaffolds in a short time. However, it only supported the printing of simple structures because the structure collapsed as the number of layers increased. Compared to cryogenic printing, FRESH printing had better printing fidelity and was not affected by the number of layers printed because the printed structure was preserved in a support bath that

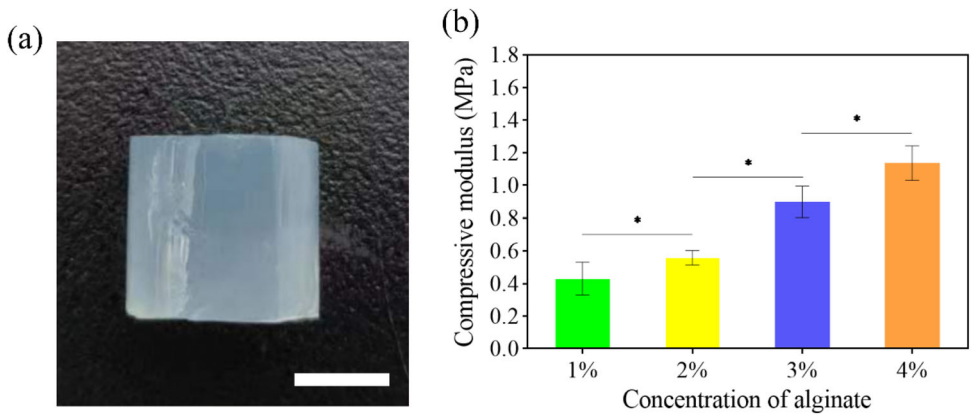

Fig. 3 **a** A hydrogel sample used in compression experiments (scale bar: 5 mm). **b** Compressive modulus of hydrogels with different concentrations of alginate. Data are represented by mean±standard deviation (n=3). $^{*}p< 0.05$

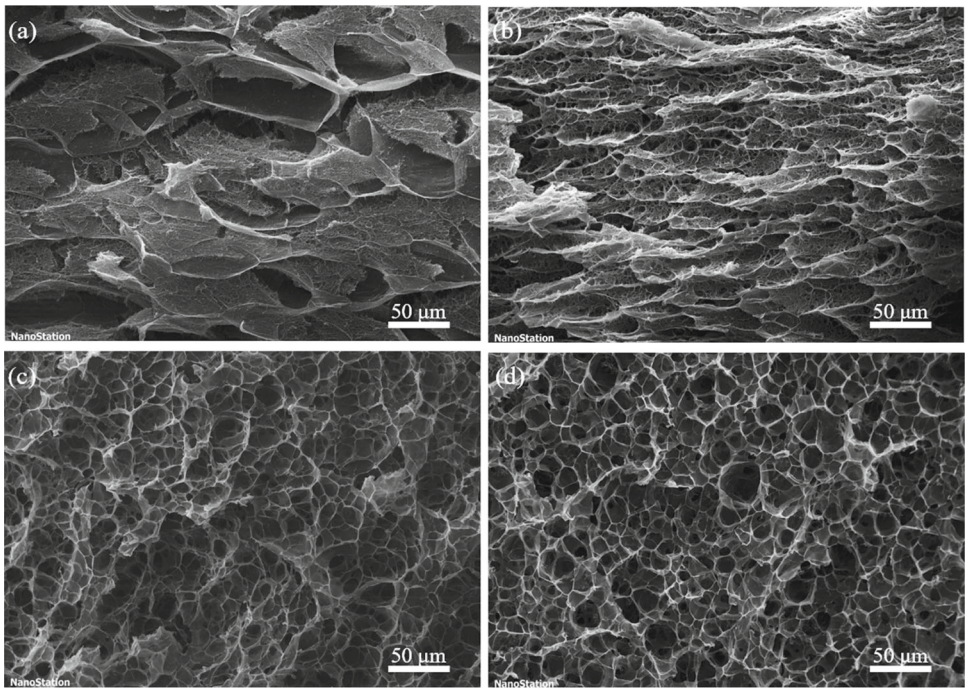

Fig. 4 Scanning electron microscopy (SEM) images to observe the porous structure of the hydrogel at gelatin concentrations of **a** 2% (0.02 g/mL), **b** 4% (0.04 g/mL), **c** 6% (0.06 g/mL), and **d** 8% (0.08 g/mL)

overcame gravity, which revealed the ability to print complex structures.

3D structure printing

To further verify the printing potential of the bioink, a series of 3D spatial structures were constructed in conjunction with the FRESH printing method, and their geometric variations were investigated. First, we printed out a continuous filamentary spiral structure with a diameter of 1 mm in the support bath (Fig. 7a). In short, the nozzle started from any point and printed a spiral structure in a single pass through continuous motion in 3D space. The printed spiral filament (Fig. 7b) had high structural precision with precise spacing between the different layers and was completely embedded in the support bath. When the structure was released from the support bath at 37 °C, the geometric shape of the initial print was still retained (Fig. 7c). Furthermore, we designed a regular tetrahedral space line structure with a side length of 1 mm (Fig. 7d). The printing path required the nozzle to print in both the upward and downward paths in the Z-axis direction (Fig. 7e). In addition, after printing half of the structure, the nozzle needed to travel emptily to connect the printed part at the last printing point and continue the printing of the other half of the structure. Subsequently, several iterations confirmed the repeatability and stability of printing, and all printed structures met the predesign requirements (Fig. 7f). This demonstrated that bioink had the ability for intermittent and repeated printing, which provided a tremendous advantage for printing complex structures.

Next, we tested the stiffness and airtightness of the printed structure. First, we designed a single thin-walled tubular structure with a radius of 2 mm and a height of 7 mm (Fig. 8a). After printing, the stability and mechanical strength

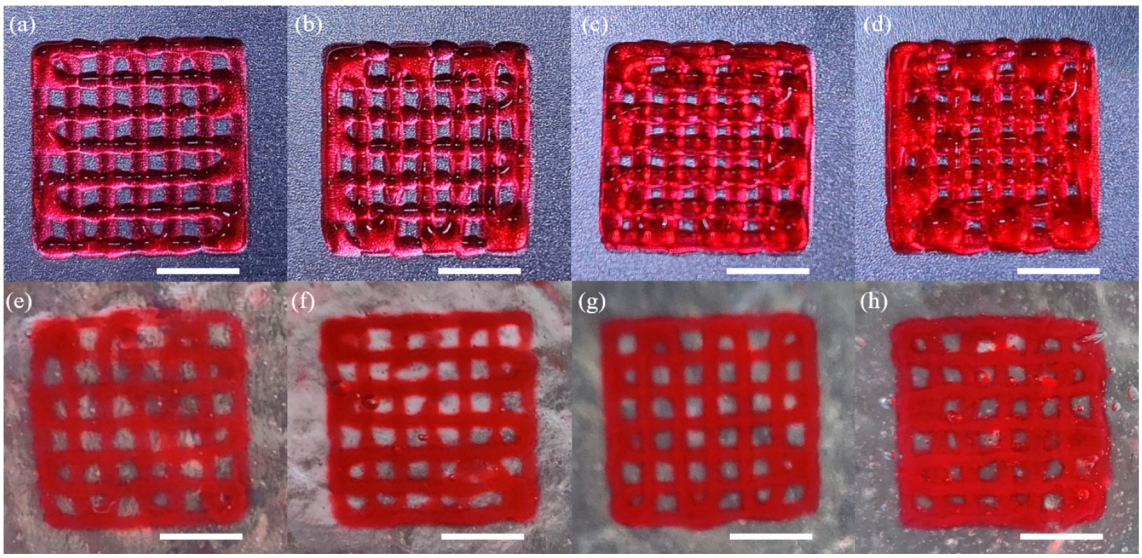

Fig. 5 Printing of multilayer lattice structures: **a**–**d** are two- to five-layer lattice structures printed on a cryogenic platform, and **e**–**h** are two- to five-layer lattice structures printed in a support bath. Scale bar: 5 mm

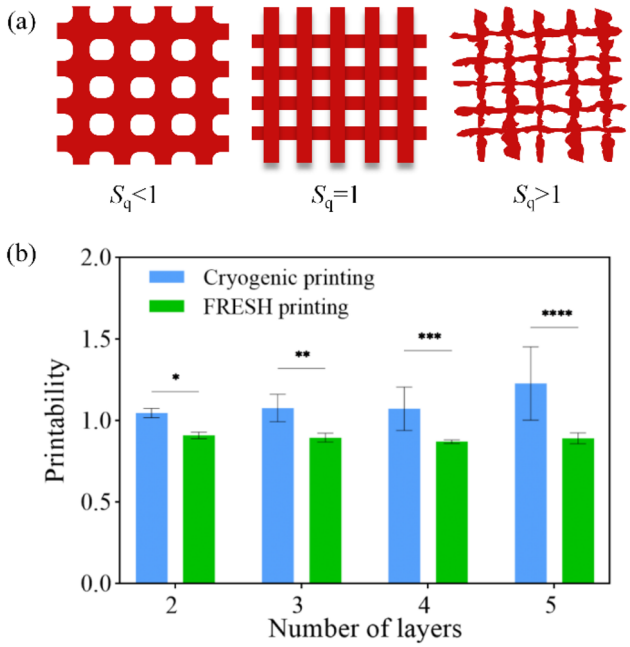

Fig. 6 **a** The printing accuracy is quantified as S_q<1 when the printed grid shrinks to a circle, S_q= 1 when the printed grid is a square, and S_q > 1 when the printed grid is an irregular polygon. **b** Printability analysis of cryogenic printing and FRESH printing methods. Data are represented by mean±standard deviation (n=3). $^{*}p$<0.05, $^{**}p$<0.01, $^{***}p$<0.001, $^{****}p$<0.0001

of the structure were tested by applying pressure to the structure several times along the radial direction. The structure returned to its original shape after pressure removal in multiple iterations of the experiment, which indicated that the printed cylindrical structure was flexible in the lateral direction. In addition, to verify the interlayer bonding of the printed structure, we printed a single-layer thin-walled tubular structure with a radius of 1 mm and a length of 15 mm (Fig. 8b). The printed results showed that all layers of the constructed circular tube were bonded to each other and could maintain the structure's stability in accordance with the designed frame. To further confirm the interlayer line fusion, we conducted perfusion experiments on the pipe with dyes, and the results showed that the tube did not produce any leakage. Finally, a model of a solid structure was designed in the shape of an "SDU" containing three parts separated from each other. The size of the model was 16.8 mm×7.08 mm× 2.00 mm. By optimizing the printing route and process, the structure was successfully printed. The model was sliced by software Slic3r and printed with 25-G nozzles. The layer thickness was set to 200 μm, and the printing speed was 100 mm/min. The whole printing process took 12 min. The printing results, shown in Fig. 8c, confirmed that bioinks could support the printing of solid split structures.

This section showed that the FRESH printing method could build complex structures using the designed bioink. FRESH printing overcame the effect of gravity in the printing process and built tissues with a low modulus, which significantly improved printing accuracy compared to previous studies [50]. It should be noted that the FRESH printing speed was limited to less than 300 mm/min; otherwise, it would cause the extruded microfilaments to uplift, resulting in print failure. Optimizing the printing parameters made the whole printing process take place in cell-friendly conditions, greatly improving the cell survival rate during the printing process.

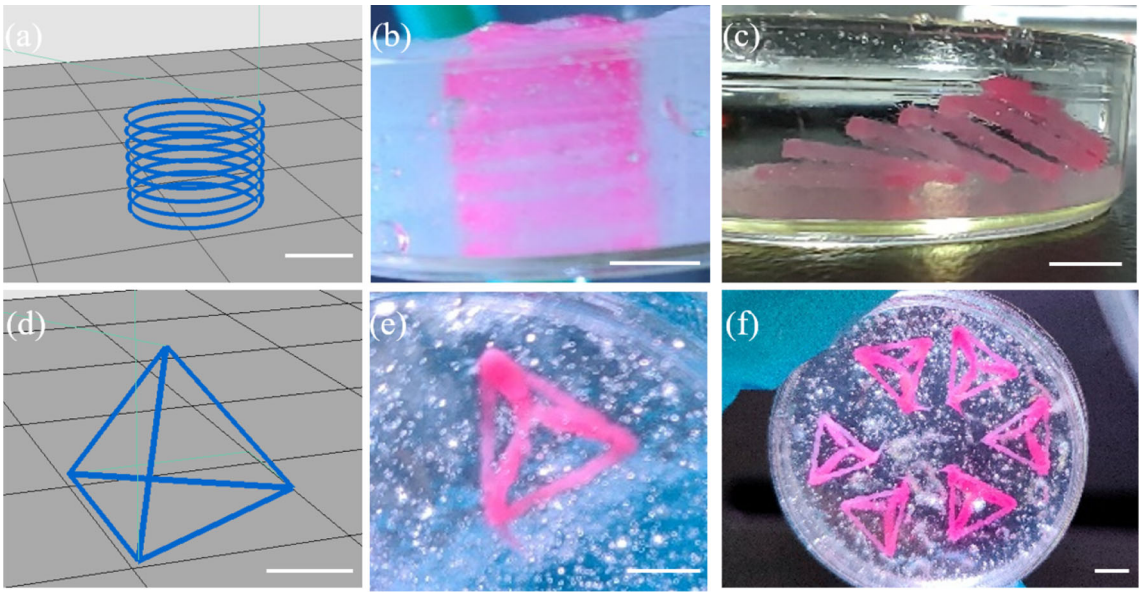

Fig. 7 Several examples of spatial printing lines. **a** and **b** are models of spatial spirals and printed entities, and **c** is the result after release from the support bath. **d** and **e** are models of regular tetrahedral space line structure and printed entities, and **f** is the figure after multiple printing. Scale bar: 5 mm

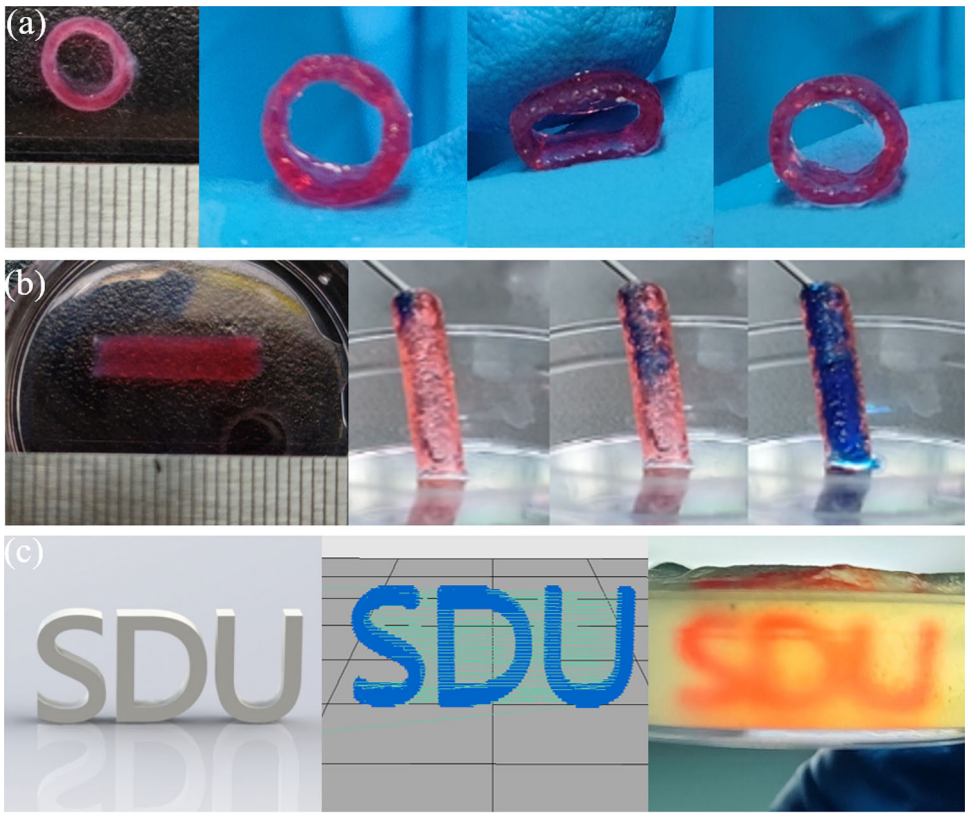

Fig. 8 Complex structures printed using FRESH. **a** The printed round tube was subjected to repeated compression experiments and recovered normally. **b** Printed elongated tube subjected to perfusion experiments with no dye leakage, indicating that the structure has good sealing properties. **c** Solid "SDU" model with dimensions of 16.8 mm×7.08 mm× 2.00 mm, sliced using Slic3r and printed in the support bath. Ruler scale: 1 mm. FRESH: freeform reversible embedding of suspended hydrogel

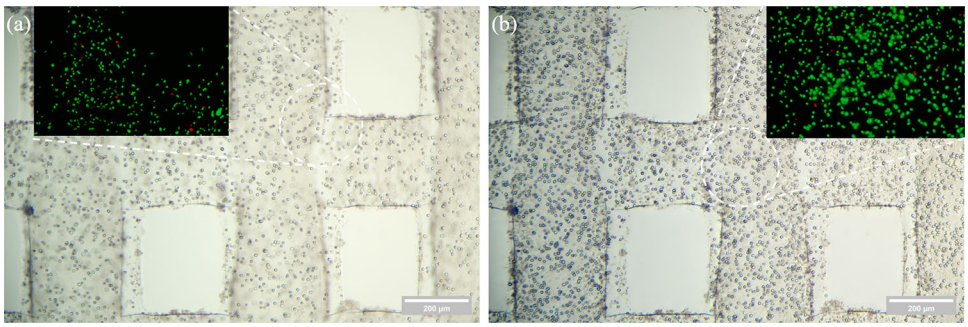

Fig. 9 Immunofluorescence staining of cells. Cell survival rates were 97.5% and 96.9% using AM/PI for staining of cells on Days 1 (**a**) and 7 (**b**) of cell culture, respectively. Live and dead cells are fluorescent green and fluorescent red, respectively. Scale bar: 200 μm. AM: acetoxymethyl ester; PI: propidium iodide

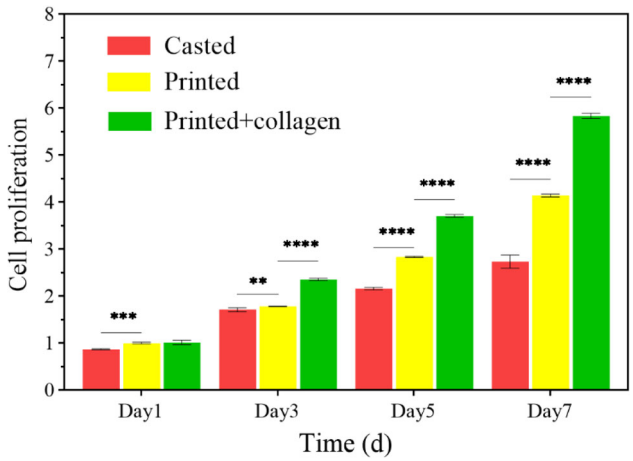

Fig. 10 Cell proliferation assays were performed on different substrates in vitro. Staining was performed using cell counting kit-8 (CCK-8) on Days 1, 3, 5, and 7 of culture. The three substrates were cast structures, printed grid structures, and printed grid structures with added collagen. Data are represented by mean±standard deviation (n=3). $^{**}p$<0.01, $^{***}p$<0.001, $^{****}p$< 0.0001

Biocompatibility of the scaffolds

The biocompatibility of the bioink was measured using L929 fibroblast cells. Specifically, a mesh structure was printed with cell-laden bioink. Cells were stained on Days 1 and 7 of culture using a live/dead staining kit to assess cell viability. Staining was observed using an inverted fluorescence microscope, as shown in Fig. 9. The live/dead cells were counted by ImageJ, and the cell survival rate was calculated to be above 96% on both Days 1 and 7. The results indicated that the printing process did not affect cell activity, and the cells maintained a high survival rate. A comparison of the microscopic images for Days 1 and 7 revealed that the number of cells grew, and the cells appeared to proliferate substantially with increasing culture time.

To further investigate the versatility of scaffold materials, we added 0.1% (0.001 g/mL) collagen as an additive to bioink to further expand the application of the bioink. Collagen exists widely in the ECM, and there is a large amount of collagen in the connective tissue of fibroblasts. However, collagen is difficult to apply in bioinks alone due to its poor solubility [51]. Specifically, we printed the scaffold structure with collagen as the additional material and compared it with the scaffolds printed without added collagen and directly cast scaffolds. The proliferation status of cells was tested with a CCK-8 kit on Days 1, 3, 5, and 7 of culture. The optical density (OD) value on the first day of the printed structure was normalized to 1. As shown in Fig. 10, cells in the three scaffolds had similar proliferation rates on the first day of culture, and the addition of collagen had no statistically significant effect on cell proliferation. As the culture progressed, the proliferation rate of cells on the three scaffolds gradually showed a noticeable difference. The perfusion scaffold was a solid structure, resulting in a poorly fluid culture medium and poor access to nutrients for the cells inside. Therefore, there was no manifested cell proliferation compared to the other two structures. The other two mesh scaffolds had an effective cell proliferation rate because the cells were evenly distributed and supported substances exchanged with the culture medium through the mesh. Furthermore, in the case of added collagen, the proliferation rate of mouse fibroblasts was twice that of the cast. In addition, studies have shown that tissue-derived bioinks (laminin, decellularized ECM) and synthetic bioinks have good biocompatibility [52, 53].

Conclusions

In summary, a cell-laden 3D-printing bioink with a tunable elastic modulus and porosity was prepared in this study. The rheological results showed that the bioink had suitable shear thinning and shear recovery properties, which would be cell-friendly during the printing process. Mechanical tests and SEM analysis revealed that the printed structures had a tunable elastic modulus and porosity. Complex soft structures were printed using the FRESH bioprinting method, which further demonstrated the promising potential of the bioink in medical applications. Cell-loaded printing was performed using L929 fibroblast cells, exhibiting high cell viability and good proliferative properties in a 7-d culture.

Collagen was added as a specific material to further promote the growth and proliferation of cells. In addition, the applicability of FRESH bioprinting with other tissue-derived bioinks (laminin, decellularized ECM) and synthetic bioinks will be investigated in future research. All the results indicated that the designed bioinks had good biological and mechanical properties, allowing the addition of cytocompatible materials, which would be a promising strategy for tissue engineering.

Acknowledgements This work was financially supported by the National Natural Science Foundation of China (Nos. 52275464 and 52075300) and the Scientific Research Project for National High-Level Innovative Talents of Hebei Province Full-Time Introduction (No. 2021HBQZYCXY004).

Author contributions ZC participated in conceptualization, investigation, methodology, and writing of the original draft. CZH was involved in supervision, conceptualization, writing—review & editing, and funding acquisition. HLL was involved in methodology. XH, ZCW, and SYL contributed to writing—review & editing. JH and ZW contributed to supervision and writing—review & editing.

Declarations

Conflict of interest CZH is an Editorial Board Member of *Bio-Design and Manufacturing*. The authors declare that they have no known competing financial interests or personal relationships that could have appeared to influence the work reported in this paper.

Ethical approval This study does not contain any studies with human or animal subjects performed by any of the authors.

Data or code availability The data generated in this study are available from the corresponding author upon reasonable request.

References

1. Zhang B, Luo Y, Ma L et al (2018) 3D bioprinting: an emerging technology full of opportunities and challenges. Bio-Des Manuf 1(1):2–13. https://doi.org/10.1007/s42242-018-0004-3
2. Ozbolat IT, Yu Y (2013) Bioprinting toward organ fabrication: challenges and future trends. IEEE Trans Biomed Eng 60(3):691–699. https://doi.org/10.1109/TBME.2013.2243912
3. Park C, Jones MM, Kaplan S et al (2022) A scoping review of inequities in access to organ transplant in the United States. Int J Equity Health 21:22. https://doi.org/10.1186/s12939-021-01616-x
4. Hurst DJ, Potter J, Padilla LA (2022) Organ transplant and Covid-19 vaccination: considering the ethics of denying transplant to unvaccinated patients. Clin Transplant 36(5):e14589. https://doi.org/10.1111/ctr.14589
5. Langer R, Vacanti JP (1993) Tissue engineering. Science 260(5110):920–926. https://doi.org/10.1126/science.8493529
6. Xu Y, Zhang F, Zhai W et al (2022) Unraveling of advances in 3D-printed polymer-based bone scaffolds. Polymers 14(3):566. https://doi.org/10.3390/polym14030566
7. Kang Y, Xu J, Meng L et al (2023) 3D bioprinting of dECM/Gel/QCS/nHAp hybrid scaffolds laden with mesenchymal stem cell-derived exosomes to improve angiogenesis and osteogenesis. Biofabrication 15(2):024103. https://doi.org/10.1088/1758-5090/acb6b8
8. Kim DH, Kim MJ, Kwak SY et al (2023) Bioengineered liver crosslinked with nano-graphene oxide enables efficient liver regeneration via MMP suppression and immunomodulation. Nat Commun 14(1):801. https://doi.org/10.1038/s41467-023-35941-2
9. Liu N, Ye X, Yao B et al (2021) Advances in 3D bioprinting technology for cardiac tissue engineering and regeneration. Bioact Mater 6(5):1388–1401. https://doi.org/10.1016/j.bioactmat.2020.10.021
10. Lawlor KT, Vanslambrouck JM, Higgins JW et al (2021) Cellular extrusion bioprinting improves kidney organoid reproducibility and conformation. Nat Mater 20(2):260–271. https://doi.org/10.1038/s41563-020-00853-9
11. Shoulders MD, Raines RT (2009) Collagen structure and stability. Annu Rev Biochem 78:929–958. https://doi.org/10.1146/annurev.biochem.77.032207.120833
12. Kumar MN, Muzzarelli RA, Muzzarelli C et al (2004) Chitosan chemistry and pharmaceutical perspectives. Chem Rev 104(12):6017–6084. https://doi.org/10.1021/cr030441b
13. Lee KY, Mooney DJ (2012) Alginate: properties and biomedical applications. Prog Polymer Sci 37:106–126. https://doi.org/10.1016/j.progpolymsci.2011.06.003
14. Arnott S, Fulmer A, Scott WE et al (1974) The agarose double helix and its function in agarose gel structure. J Mol Biol 90(2):269–284. https://doi.org/10.1016/0022-2836(74)90372-6
15. Yu K, Zhang X, Sun Y et al (2021) Printability during projection-based 3D bioprinting. Bioact Mater 11:254–267. https://doi.org/10.1016/j.bioactmat.2021.09.021
16. Gungor-Ozkerim PS, Inci I, Zhang YS et al (2016) Bioinks for 3D bioprinting: an overview. Biomater Sci 6(5):915–946. https://doi.org/10.1039/c7bm00765e
17. He Y, Yang F, Zhao H et al (2016) Research on the printability of hydrogels in 3D bioprinting. Sci Rep 6:29977. https://doi.org/10.1038/srep29977
18. Skeldon G, Lucendo-Villarin B, Shu W (2018) Three-dimensional bioprinting of stem-cell derived tissues for human regenerative medicine. Phil Trans R Soc B 373(1750):20170224. https://doi.org/10.1098/rstb.2017.0224
19. Hölzl K, Lin S, Tytgat L et al (2016) Bioink properties before, during and after 3D bioprinting. Biofabrication 8(3):032002. https://doi.org/10.1088/1758-5090/8/3/032002
20. Pati F, Jang J, Ha DH et al (2014) Printing three-dimensional tissue analogues with decellularized extracellular matrix bioink. Nat Commun 5:3935. https://doi.org/10.1038/ncomms4935
21. Corbett DC, Olszewski E, Stevens K (2019) A FRESH take on resolution in 3D bioprinting. Trends Biotechnol 37(11):1153–1155. https://doi.org/10.1016/j.tibtech.2019.09.003
22. Balmforth NJ, Frigaard IA, Ovarlez G (2014) Yielding to stress: recent developments in viscoplastic fluid mechanics. Annu Rev Fluid Mech 46:121–146. https://doi.org/10.1146/annurev-fluid-010313-141424
23. Hinton TJ, Hudson A, Pusch K et al (2016) 3D printing PDMS elastomer in a hydrophilic support bath via freeform reversible embedding. ACS Biomater Sci Eng 2(10):1781–1786. https://doi.org/10.1021/acsbiomaterials.6b00170
24. O'Bryan CS, Bhattacharjee T, Hart S et al (2017) Self-assembled micro-organogels for 3D printing silicone structures. Sci Adv 3(5):e1602800. https://doi.org/10.1126/sciadv.1602800
25. Colly A, Marquette C, Courtial EJ (2021) Poloxamer/poly(ethylene glycol) self-healing hydrogel for high-precision freeform reversible embedding of suspended hydrogel. Langmuir 37(14):4154–4162. https://doi.org/10.1021/acs.langmuir.1c00018
26. Lee A, Hudson AR, Shiwarski DJ et al (2019) 3D bioprinting of collagen to rebuild components of the human heart. Science 365(6452):482–487. https://doi.org/10.1126/science.aav9051
27. Mirdamadi E, Tashman JW, Shiwarski DJ et al (2020) FRESH 3D bioprinting a full-size model of the human heart. ACS

Biomater Sci Eng 6(11):6453–6459. https://doi.org/10.1021/acsbiomaterials.0c01133
28. Zhang Z, Wu C, Dai C et al (2022) A multi-axis robot-based bioprinting system supporting natural cell function preservation and cardiac tissue fabrication. Bioact Mater 18:138–150. https://doi.org/10.1016/j.bioactmat.2022.02.009
29. Lan X, Liang Y, Erkut EJN et al (2021) Bioprinting of human nasoseptal chondrocytes-laden collagen hydrogel for cartilage tissue engineering. FASEB J 35(3):e21191. https://doi.org/10.1096/fj.202002081R
30. Ostrovidov S, Salehi S, Costantini M et al (2019) 3D bioprinting in skeletal muscle tissue engineering. Small 15(24):1805530. https://doi.org/10.1002/smll.201805530
31. Hinton TJ, Jallerat Q, Palchesko RN et al (2015) Three-dimensional printing of complex biological structures by freeform reversible embedding of suspended hydrogels. Sci Adv 1(9):e1500758. https://doi.org/10.1126/sciadv.1500758
32. Shiwarski DJ, Hudson AR, Tashman JW et al (2021) Emergence of FRESH 3D printing as a platform for advanced tissue biofabrication. APL Bioeng 5:010904. https://doi.org/10.1063/5.0032777
33. Paxton N, Smolan W, Böck T et al (2017) Proposal to assess printability of bioinks for extrusion-based bioprinting and evaluation of rheological properties governing bioprintability. Biofabrication 9(4):044107. https://doi.org/10.1088/1758-5090/aa8dd8
34. Lindsay CD, Roth JG, LeSavage BL et al (2019) Bioprinting of stem cell expansion lattices. Acta Biomater 95:225–235. https://doi.org/10.1016/j.actbio.2019.05.014
35. Lewicki J, Bergman J, Kerins C et al (2019) Optimization of 3D bioprinting of human neuroblastoma cells using sodium alginate hydrogel. Bioprinting 16:e00053. https://doi.org/10.1016/j.bprint.2019.e00053
36. Kozlov PV, Burdygina GI (1983) The structure and properties of solid gelatin and the principles of their modification. Polymer 24:651–666. https://doi.org/10.1016/0032-3861(83)90001-0
37. Yang F, Tadepalli V, Wiley BJ (2017) 3D printing of a double network hydrogel with a compression strength and elastic modulus greater than those of cartilage. ACS Biomater Sci Eng 3(5):863–869. https://doi.org/10.1021/acsbiomaterials.7b00094
38. Sun M, Sun X, Wang Z et al (2018) Synthesis and properties of gelatin methacryloyl (GelMA) hydrogels and their recent applications in load-bearing tissue. Polymers 10(11):E1290. https://doi.org/10.3390/polym10111290
39. Hoch E, Hirth T, Tovar GEM et al (2013) Chemical tailoring of gelatin to adjust its chemical and physical properties for functional bioprinting. J Mater Chem B 1(41):5675–5685. https://doi.org/10.1039/C3TB20745E
40. Blaeser A, Duarte Campos DF, Puster U et al (2016) Controlling shear stress in 3D bioprinting is a key factor to balance printing resolution and stem cell integrity. Adv Healthc Mater 5(3):326–333. https://doi.org/10.1002/adhm.201500677
41. Engler AJ, Sen S, Sweeney HL et al (2006) Matrix elasticity directs stem cell lineage specification. Cell 126(4):677–689. https://doi.org/10.1016/j.cell.2006.06.044
42. Huebsch N, Arany PR, Mao AS et al (2010) Harnessing traction-mediated manipulation of the cell/matrix interface to control stem-cell fate. Nat Mater 9(6):518–526. https://doi.org/10.1038/nmat2732
43. Carrow JK, Kerativitayanan P, Jaiswal MK et al (2015) Polymers for bioprinting. In: Atala A, Yoo JJ (Eds.), Essentials of 3D Biofabrication and Translation. Academic Press, Boston, USA, p.229–248. https://doi.org/10.1016/B978-0-12-800972-7.00013-X
44. Leipzig ND, Shoichet MS (2009) The effect of substrate stiffness on adult neural stem cell behaviour. Biomaterials 30(36):6867–6878. https://doi.org/10.1016/j.biomaterials.2009.09.002
45. Lee W, Pinckney J, Lee V et al (2009) Three-dimensional bioprinting of rat embryonic neural cells. NeuroReport 20(8):798–803. https://doi.org/10.1097/WNR.0b013e32832b8be4
46. Hu X, Wang Y, Zhang L et al (2021) Simple ultrasonic-assisted approach to prepare polysaccharide-based aerogel for cell research and histocompatibility study. Int J Biol Macromol 188:411–420. https://doi.org/10.1016/j.ijbiomac.2021.08.034
47. Ghafari R, Jonoobi M, Amirabad LM et al (2019) Fabrication and characterization of novel bilayer scaffold from nanocellulose based aerogel for skin tissue engineering applications. Int J Biol Macromol 136:796–803. https://doi.org/10.1016/j.ijbiomac.2019.06.104
48. Shao L, Gao Q, Xie C et al (2020) Sacrificial microgel-laden bioink-enabled 3D bioprinting of mesoscale pore networks. Bio-Des Manuf 3(1):30–39. https://doi.org/10.1007/s42242-020-00062-y
49. Wang Z, Huang C, Han X et al (2022) Fabrication of aerogel scaffolds with adjustable macro/micro-pore structure through 3D printing and sacrificial template method for tissue engineering. Mater Des 217:110662. https://doi.org/10.1016/j.matdes.2022.110662
50. Chung JHY, Naficy S, Yue Z et al (2013) Bio-ink properties and printability for extrusion printing living cells. Biomater Sci 1(3):763–773. https://doi.org/10.1039/C3BM00012E
51. Moncal KK, Ozbolat V, Datta P et al (2019) Thermally-controlled extrusion-based bioprinting of collagen. J Mater Sci Mater Med 30:55. https://doi.org/10.1007/s10856-019-6258-2
52. Kreimendahl F, Kniebs C, Sobreiro AMT et al (2021) FRESH bioprinting technology for tissue engineering – the influence of printing process and bioink composition on cell behavior and vascularization. J Appl Biomater Funct Mater 19:1–11. https://doi.org/10.1177/22808000211028808
53. Ahn M, Cho WW, Kim BS et al (2022) Engineering densely packed adipose tissue via environmentally controlled in-bath 3D bioprinting. Adv Funct Mater 32:2200203. https://doi.org/10.1002/adfm.202200203